EXERGETIC PERFORMANCE EVALUATION OF OCEAN THERMAL ENERGY CONVERSION SYSTEM WITH CROSSFLOW PLATE HEAT EXCHANGERS

Takeshi Yasunaga*, Taisei Nakamura, Tomoya Okuno, Yasuyuki Ikegami

*Institute of Ocean Energy, Saga University, Japan
1 honjo-machi, Saga city, Saga 8408502, Japan

*Corresponding Author: yasunaga@ioes.saga-u.ac.jp

ABSTRACT

Ocean thermal energy conversion (OTEC) systems can convert the ocean thermal energy stored as a vertical temperature gradient in the ocean to electricity. Because the temperature difference in the heat engine is low, zeotropic mixtures and staging heat engines are applied to increase the power output. Recently, we proposed a method to evaluate the performance of the OTEC to identify the irreversible loss and energy conversion efficiency based on finite-time thermodynamics (FTT). In particular, this approach can determine the irreversible loss in the heat balance design and heat exchange process, and this concept can be extended to consider the internal irreversibility of heat engines. In this work, the performance of a single Rankine cycle OTEC with a crossflow plate heat exchanger as an evaporator and a condenser was experimentally evaluated to clarify the irreversibility of the heat engine and exergy. The internal irreversibility of the heat engine and effect of the staging of the heat engine were discussed. Moreover, the experimental results for the simple Rankine framework were extended to the numerical simulation of a two-stage Rankine cycle to compare the effect of the staging configuration such as cascade or parallel installations. The maximum net exergy efficiency reached 26%, 30% and 40% in the single Rankine cycle, parallel two-unit Rankine cycle and cascade double-stage Rankine cycle, respectively. The results demonstrate that the FTT model can effectively realize performance evaluation and can be applied to achieve optimal control and design.

1 INTRODUCTION

Ocean thermal energy conversion (OTEC) systems represent one of the lowest-grade thermal energy conversion systems that can convert sensible heat, which is the temperature difference between the surface seawater (approximately 30 °C) and deep seawater (approximately 5–10 °C), to work. The potential energy of OTEC systems is large, and thus, such systems are primarily applied in tropical oceans (IEA-OES, 2019). In the Okinawa prefecture Deep Ocean Water Research Center, Kumejima, Okinawa, Japan, an ORC OTEC demonstration plant using R134a has been operating since 2013 and currently has a generation capacity of 100 kW. Moreover, a 105 kW OTEC plant located at the Ocean Energy Research Center in Kona, Hawaii, USA, has been operating since 2015. In both these projects, the deep ocean water is used as a resource for many industries such as aquaculture for shrimps and umibudo, agriculture for cooling soils, mineral water production, and cosmetics (Martine et al., 2016).In addition, a 1 MW OTEC was tested near the coast of Busan, Korea by KRISO, Korea in 2019, and the system generated a power of 338 kW by exploiting the temperature difference of 24.8 °C and 6.1 °C (IEA-OES, 2019).

In conventional thermal power plants, the design constraint of the turbine inlet steam temperature pertains to the thermal-resistant materials on the boilers against the combustion temperature. Specifically, the combustion temperature is higher than the current turbine inlet steam temperature. Owing to the large difference between the heat source combustion temperature and temperature of the heat engine, an increase in the turbine inlet steam temperature enhances the thermal efficiency of the heat engine. In contrast, OTEC heat engines are driven by an extremely small temperature difference of approximately 20–25 °C. Therefore, the heat transfer rate from the heat source and temperature

difference to operate the heat engine are key aspects to maximize the available work from the heat engine. In this context, it is necessary to ensure the balance of the heat source temperature change and turbine inlet/outlet temperatures. Wu (1987) first applied the finite-time thermodynamics (FTT) technique to the OTEC system assuming an infinite mass flow rate of the seawater and finite heat transfer performance of the heat exchangers between the heat source and Carnot heat engine. It was noted that the thermal efficiency pertaining to the maximum work corresponded to the Curzon–Ahlborn thermal efficiency $\eta_{th,CA}$, known as the upper bound of the thermal efficiency expressed using warm surface seawater temperature T_W and cold deep seawater T_C as follows:

$$\eta_{th,CA} = \sqrt{\frac{T_C}{T_W}} \tag{1}$$

Ikegami and Bejan (1998) considered the Carnot cycle and infinite heat transfer performance of heat exchangers and defined the thermal efficiency at the maximum net power as the difference between the gross power and total seawater pumping power. Moreover, the authors extended the concept of FTT modeling to OTEC considering the finite heat transfer performance and finite flow rate of the heat source, considering an ideal heat engine (Yasunaga and Ikegami, 2020a) and irreversibility of the heat engine (Yasunaga and Ikegami, 2020b). In particular, FTT modeling can be easily used to evaluate the power generation system through the normalized thermal efficiency and exergy efficiency (Yasunaga et al., 2021), to control the maximization of the available power, and to perform design optimization and performance evaluation of components such as heat exchangers (Yasunaga et al, 2018, and Fontaine, et al., 2019) and working fluids in the case of ORC (Yasunaga and Ikegami, 2019). Although the traditional parametric analysis (Uehara and Ikegami, 1990) and optimization (Owens, 1983, Uehara and Nakaoka, 1985, 1987) techniques provide a more precise design heat balance, including the heat exchanger specification to maximize the available net power per heat transfer area, the calculation method is complicated. Moreover, the actual plant design involves certain design margins for each equipment and the total system; therefore, the maximum condition is different from the design condition. Whereas, the FTT model is easy for manipulation of the control parameter such as heat source and working fluid mass flow rate to achieve the maximum condition while the plant is operating. In such scenarios, the FTT model can be adapted to the maximum net power condition.

Yasunaga and Ikegami (2020b) experimentally validated the FTT model using a 30 kW OTEC experimental apparatus with shell-and-plate and frame-and-plate type heat exchangers with a counter flow. In their research, the constant overall irreversibility coefficient was applied in the limited operating condition to identify the optimum operating condition, and the net exergy efficiency was noted to be approximately 10%. Furthermore, the application of a zeotropic mixture working fluid and staging heat engine was noted to theoretically increase the exergy and available net power in the power generation system (Kalina, 1995, Ikeami, et al., 2018, Yasunaga et al., 2021).

In this study, first, the FTT model was constructed for an OTEC experimental apparatus to identify the optimum operating condition. Second, the influence of the staging on the net power at the same total seawater flow rate was investigated by comparing the results of the single-stage Rankine cycle, double-stage Rankine cycle, and double-capacity Rankine cycle by using the FTT model established based on a single-stage Rankine cycle.

2 FTT MODEL FORMULATION

In an OTEC system, the thermal energy pertaining to the difference between the warm seawater temperature T_W and cold deep seawater temperature T_C is transferred to a heat engine to produce work W. The energy conservation in the energy conversion process, involving the heat transfer of Q_W to the heat engine to convert the thermal energy into W and the discharge heat transfer of Q_C, along with each thermal energy can be calculated using the following expressions:

$$W = Q_W - Q_C \tag{2}$$

$$Q_W = C_W\left(T_W - T_{W,O}\right) = \left(UA\Delta T_m\right)_{Eva} \tag{3}$$

$$Q_C = C_C\left(T_{C,O} - T_C\right) = \left(UA\Delta T_m\right)_{Con} \tag{4}$$

where C is the heat capacity flow rate, which is the product of the mass flow rate and specific heat, T is the temperature, U is an overall heat transfer coefficient (kW/(m^{2}K)), A is the heat transfer area of the heat exchanger (m^2), and ΔT_m is the logarithmic mean temperature difference; subscripts W and C denote the surface and deep seawater, respectively; subscripts *Eva, Con* and *O* indicate the evaporator, condenser, and outlet, respectively.

The total entropy production in the energy conversion process, S_{gen}, is the sum of the total heat leak from the heat engine, $\Sigma S_{heat\text{-}leak}$, irreversibility caused by the finite heat transfer performance of the heat exchangers, $\Sigma S_{heat\text{-}transfer}$, irreversibility of the heat engine during the energy conversion, $S_{heatngine}$, and parasitic power (back work) corresponding to the seawater pumping power in the system, $\Sigma S_{back\text{-}work}$.

$$S_{gen} = \Sigma S_{heat-leak} + \Sigma S_{heat-transfer} + \Sigma S_{heat-engine} + \Sigma S_{back-work} > 0 \tag{5}$$

Herein, the power generation system includes the seawater intake, delivery, and discharge processes; energy conversion process to convert the thermal energy into work; and heat exchange process. In the power generation system, the minimization of $\Sigma S_{heat\text{-}leak}$ corresponds to the maximization of the work in the heat engine, i.e., maximization of the power production in the system.

Therefore, when using an ideal heat engine, the minimization of $\Sigma S_{heat\text{-}leak}$ corresponds to the exergy of the heat source, Ex_{OTEC} (Yasunaga and Ikegami, 2020).

$$Ex_{OTEC} = C_W T_W + C_C T_C - (C_W + C_C) T_W^{\left(\frac{C_W}{C_W + C_C}\right)} T_C^{\left(\frac{C_C}{C_W + C_C}\right)} \tag{6}$$

The entropy production in the heat exchange process consists of two performance values, specifically, the finite heat transfer performance that causes the finite temperature difference between the heat exchangers and heat engine, and the pressure drop associated with the fluid flow. In general, the performance of a heat exchanger is evaluated in terms of the heat transfer performance; thermal resistances pertaining to the heat transfer coefficients and thermal conductivity and thickness of the heat exchanger materials; and pressure drops due to the fluid flow. The amount of entropy generation can be calculated considering these performance aspects in the exergy analysis. However, in this study, the objective of the evaluation is the net power output in the power generation system. In other words, the effective temperature difference available to a heat engine is determined considering the heat transfer performance of the heat exchanger. In this scenario, the pressure drop due to the flow on the heat source side generates back work in the system, and the pressure drop on the working fluid side deteriorates the performance of power generation. This loss is considered as the irreversibility pertaining to the heat engine. Therefore, the performance of the heat exchanger affects each of the second to fourth terms on the right-hand side in Equation (5).

The overall irreversibility coefficient for the heat engine ϕ (<1) can be defined as follows (Yasunaga and Ikegami, 2020).

$$S_{in} - \phi S_{out} = 0 \tag{7}$$

where ϕ takes into account the expansion (turbine) and compression (working fluid pump) processes as well as the pressure drop in piping and valves due to the working fluid flow in the heat engine, and heat transfer performance of exchanger exchangers. The maximum work obtained from the heat engine is determined by minimizing the first and third terms on the right-hand side in Equation (5),

$$W_{m,NTU,\phi} = \frac{\phi C_C C_W \varepsilon_{Con} \varepsilon_{Eva} \left(\sqrt{T_{W,I}} - \sqrt{T_{C,I}/\phi}\right)^2}{\phi C_C \varepsilon_{Con} + C_W \varepsilon_{Eva}} \tag{8}$$

where ε is the heat transfer performance effectiveness defined in terms of the net transfer unit (*NTU)*. $W_{m,NTU,\phi}$ is equivalent to the work from heat engine W in the energy conservation in Eq.(2), which express the net power of heat engine meaning turbine powers minus working pump loads.

$$\varepsilon_{Eva} = 1 - e^{-NTU_{Eva}}\ ,\ \varepsilon_{Con} = 1 - e^{-NTU_{Con}} \tag{9}$$

$$NTU = \frac{UA}{C} \tag{10}$$

Considering $S_{back\text{-}work}$, due to the pumping power of the warm and cold sources, the net power output of the power generation system at maximum work, $W_{m,NTU,\phi,net}$, is

$$W_{m,NTU,\phi,net} = W_{m,NTU,\phi} - P_W - P_C = \frac{\phi C_C C_W \varepsilon_{Con}\varepsilon_{Eva}\left(\sqrt{T_{W,I}}-\sqrt{T_{C,I}/\phi}\right)^2}{\phi C_C \varepsilon_{Con}+C_W \varepsilon_{Eva}} - \left(\frac{m\Delta p}{\rho\,\eta_P}\right)_W - \left(\frac{m\Delta p}{\rho\,\eta_P}\right)_C \quad (11)$$

where P is the pumping power (kW), Δp is the pressure drop (kPa), and η_P is the pump efficiency. Eq. (11) based on FTT shows the maximum available power in the OTEC system with a heat engine of single temperature level. For the performance analysis of an OTEC system, the comparison between the achieved power and Eq. (11) gives understandings how the system destructs the exergy. Specially, dividing the exergy destructs into each heat exchanger performance, the irreversibility of heat engine, and required power to collect the thermal energy of the ocean by pumping seawater. This analysis is a useful tool for not only the performance analysis but also the design optimization of the system.

3 EXPERIMENTAL APPARATUS AND CONDITIONS

3.1 OTEC Experimental Apparatus

Figure 1 (a) shows the schematic of the process flow of the OTEC experimental apparatus using a single-stage Rankine cycle (S-R), and Figure 1 (b) shows the picture of the experimental apparatus. The experimental apparatus consists of an evaporator, a gas–liquid separator, a condenser, a pressure reduction valve, working fluid pump and heat source pumps. The working fluid liquid is pumped to the evaporator and vaporized in the evaporator through heating by warm water. The vapor is decompressed in the pressure reduction valve. The decompressed vapor is input to the condenser to be liquefied through cooling with cold water. If the outlet of the evaporator involves a vapor/liquid two phase, the gas–liquid separator is used to separate the mixture into single phases, and the liquid circulates to the evaporator again. Instead of the turbine/generator, the pressure reduction valve produces a pressure difference to simulate the turbine to operate in the wide range of the condition and to minimize the effect of the turbine/generator performance in variable condition to study the fundamental characteristics of the heat engine. Nevertheless, the valve cannot convert the fluid energy to work, and thus, the enthalpy balance is the same at the inlet and outlet of turbine. The warm and cold water, the temperatures of which are controlled using boilers and a refrigerator, respectively, are used as the heat sources. Table 1 shows the summary of the uncertainty of measurement. Temperature and pressure are measured by platinum resistance temperature detectors and absolute pressure transmitter and pressure difference transmitters at inlet and outlet of the components including pressure reduction valve. And water flow rates are measured by magnetic flow meters at before entering the heat exchangers, and the working fluid flow rate is measured by Coriolis flow meter at the locations shown in Figure 1 (a). The pressure difference of heat exchangers is measured at inlet/outlet of the heat exchangers. The pure ammonia is used as the working fluid since ammonia is the most suitable working fluid in terms of the power generation because of high heat transfer performance and low cost (Avery and Wu, 1994, Vera, et al, 2020), and, then, current research focus on the pure working fluid. REFPROP (Ver.10.0) was employed to calculate the fluid thermophysical properties of ammonia (Lemmon, et al., 2018).

3.2 Experimental Conditions

The experimental conditions are summarized in Table 2. The cold water inlet temperature, flow rate, and working fluid flow rate were set as 9 °C, 37 kg/s, and 0.38 kg/s, respectively. The warm water inlet temperature and flow rate were varied in the range of 29–31 °C and 20–50 kg/s in increments of 1 °C and 10 kg/s, respectively. The data acquisition sampling period was 1 Hz, and the average data for the last 30 min of each 40 min slot, corresponding to steady-state operation, was considered in the

Table 1:Summary of the uncertainty of measurement

Parameter	Range	Uncertainty	
		Absolute value	Relative value (%)
Temperature	0–50 °C	± 0.1 °C	± 0.20
Working fluid pressure	0–2000 kPa	± 5.0 kPa	± 0.25
Water pressure difference	-50–50 kPa	± 10 kPa	± 0.10
Working fluid flow rate	0–1.39 kg/s	± 0.42×10^{-3} kg/s	± 0.11
Water flow rate	0–300 m^3/h	± 1.5 m^3/h	± 0.50

performance analysis. The steady-state condition in this research is defined as follows, by monitoring the history of heat source and working fluid temperature, flow rates and pressures, and if these parameters becomes stable, we kept the heat source temperatures with a margin of errors of plus or minus 0.2 K, and working fluid flow rate with a margin of error of plus or minus 0.02 kg/s.
The specifications of the heat exchangers are presented Table 3. The evaporator and condenser had the same specifications. The plate had a height and width of 2.4 m and 0.71 m, respectively, and 48 plates were packed in the heat exchanger with a total heat transfer area of 87.4 m^2. To ensure resistance to seawater, titanium plates were adopted, and all the plates were welded to avoid any ammonia leakage. The warm and cold water flowed horizontally, whereas the working fluid flowed vertically upward and downward in the evaporator and condenser, respectively.

3.3 Performance Analysis

The output of the heat engine (W_T-P_{WF}) and net power output W_{net} were calculated using the following equations:

$$W_T - P_{WF} = \eta_T m_{WF}\left(h_{T,I} - h_{T,O}\right) - \left[\frac{m_{WF}\left(h_{P,O}-h_{P,I}\right)}{\eta_{WF,P}}\right] \tag{12}$$

$$W_{net} = W_T - P_{WF} - (P_W + P_C) = W_T - P_{WF} - \left(\frac{m\Delta p}{\rho\eta_P}\right)_W - \left(\frac{m\Delta p}{\rho\eta_P}\right)_C \tag{13}$$

where P is the pump workload, h is the specific enthalpy, η is the efficiency, m is the mass flow rate, and Δp is the pressure drop in the heat source. The subscripts WF, T, and P denote the working fluid, turbine, and pump, respectively. The specific enthalpy at the turbine inlet $h_{T,I}$ was calculated considering the pressure at the evaporator outlet, assuming that the state corresponded to saturated vapor. The specific enthalpy at the turbine outlet $h_{T,O}$ was calculated using the turbine outlet pressure and isentropic entropy at the turbine inlet. The inlet and outlet specific enthalpies of the working fluid pump, $h_{P,I}$ and $h_{P,O}$, respectively, were calculated from the measured temperature and pressure values at each point. The working fluid flow rate m_{WF} was measured at the working fluid pump outlet. The turbine efficiency η_T was assumed to be 65% in all the experimental conditions. In Equation (13), Δp was considered to be the pressure difference between only the inlet and outlet of the heat exchangers including the headers, i.e., the pressure drop in the piping system was neglected. The efficiency η_P of the heat source intake pumps P_W and P_C was assumed to be 85%. To evaluate the performance of the power generation system, the net exergy efficiency $\eta_{ex,net}$ was defined using Equations (6) and (13):

$$\eta_{ex,net} = \frac{W_{net}}{Ex_{OTEC}} \tag{14}$$

Talluri, et al. (2021) and Dincer et al. (2021) apply conventional exergy analysis technique using ambient temperature and to analysis the performance of component as well as exergo-economic analysis. The reason why current research applies Eq. (14) instead of the conventional exergy analysis is the dependency of the exergy on the ambient temperature, although OTEC uses cold deep seawater that is less than ambient temperature. Additionally, although Yasunaga and Ikegami (2020a) shows that the conventional exergy definition agrees in principal with the maximum available work in Eq. (6) when the conventional exergy uses the equilibrium temperature between the warm seawater and cold seawater,

$$U = Q/(\Delta T_m A) \tag{15}$$

$$(\Delta T_m)_{Eva} = \frac{(T_W - T_{Eva,I}) - (T_{W,O} - T_{Eva,O})}{\ln[(T_W - T_{Eva,I})/(T_{W,O} - T_{Eva,O})]}, (\Delta T_m)_{Con} = \frac{(T_{Con,I} - T_C) - (T_{Con,O} - T_{C,O})}{\ln[(T_{Con,I} - T_C)/(T_{Con,O} - T_{C,O})]} \tag{16}$$

Table 2: Experiment conditions of the heat source

Item	Value
Warm source inlet temperature (°C)	29, 31
Cold source inlet temperature (°C)	9
Warm source flow rate (kg/s)	20–50
Cold source flow rate (kg/s)	37
Working fluid flow rate (kg/s)	0.38

Table 3: Specifications of the heat exchangers

Parameter	**Value**
Structure	Frame
Length (mm)	2400
Width (mm)	709
Plate clearance (mm)	2.8
Number of plates	48
Heat transfer area (m^2)	87.4

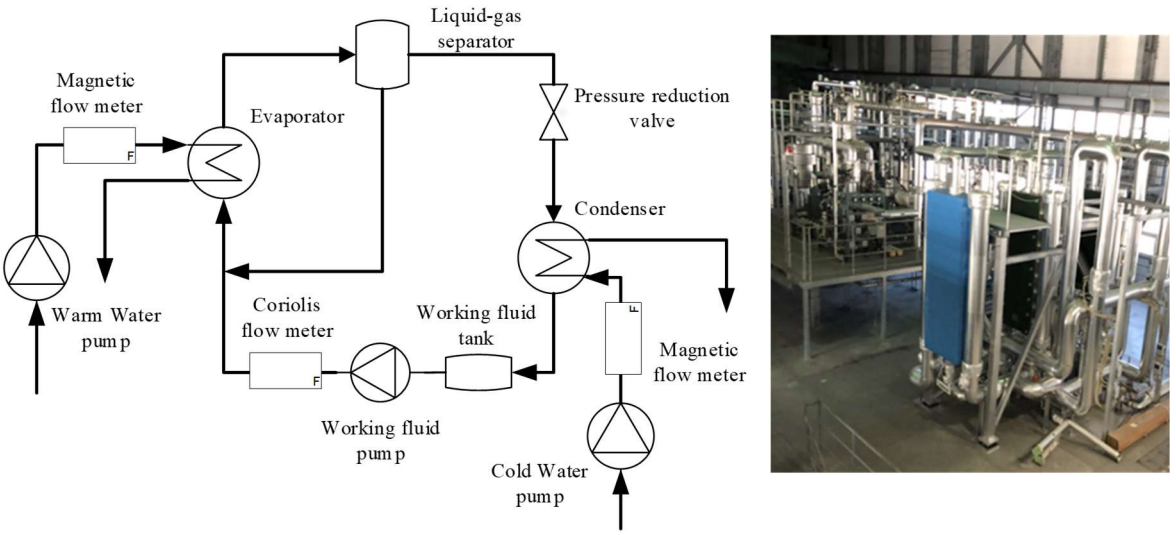

(a) Flow diagram (b) Picture of the apparatus

Figure 1: OTEC experimental apparatus using the Rankine cycle with ammonia as the working fluid

the FTT model is easy to analyze the effect of the performance of the component on the net power (Bejan, A., 2016). However, the understanding of the difference between the conventional exergy and the current FTT model in OTEC shall be discussed in another research topic.
In the heat exchanger performance evaluation, the overall heat transfer coefficient U was calculated using Equations (2) and (3).

4 FTT MODELING AND STAGING EFFECT

4.1 Overall Irreversibility in the Heat Engine and Heat Exchanger Performance

In general, the power output of the heat engine increases in proportion to the increase in C_W, which is the product of the mass flow rate and specific heat, obtained according to the maximum power output of the heat engine using Equation (8). In contrast, the pump workload increases as the cubic function of the mass flow rate. Owing to these parameters, the net power output exhibits a maximum point (Ikegami and Bejan, 1995, Yasunaga and Ikegami, 2020b).
Figure 2 shows the experimental results of (W_T - P_{WF}), (P_W +P_C), and W_{net} with uncertainty bands as a function of the mass flow rate of warm heat source m_W. According to Figure 2, as m_W increases, (W_T - P_{WF}) increases proportionally, and (P_W +P_C) increases logarithmically. Moreover, W_{net} exhibits a gradual curve, with values ranging from 9.3–10.4 kW and from 10.5–11.8 kW at 29 °C and 31 °C, respectively.
The FTT modeling can effectively clarify the optimum operating condition of the mass flow rate of the warm water and performance associated with the maximum net power condition. To calculate the net power specified in Equation (13) by using theoretical maximum power specified in Equation (11), simplified empirical formulas of the heat exchanger performance and overall irreversibility must be adopted. In the FTT model shown in Equation (11), the pressure drops in all the piping system to convey the seawater for intake and discharge are neglected as same as experimental analysis.
Figure 3 shows the overall heat transfer coefficient of the evaporator, U_{Eva}, and the pressure drop in the warm heat source side, Δp. The overall heat transfer coefficient is a function of the forced convection heat transfer coefficient of the warm heat source, which mainly depends on the Reynolds number of the warm heat source; boiling heat transfer coefficient; thermal conductivity and thickness of the plate; and thermal resistance due to fouling. In general, the heat transfer coefficient of the warm heat source is the dominant parameter in the overall heat transfer coefficient in the evaporator. Additionally, the pressure drop of warm heat source is a function of the Reynolds number. Therefore, to model the FTT in this research, U_{Eva} is simplified as a function of m_W:

$$U_{Eva} = 0.812 {m_W}^{0.310} \tag{17}$$

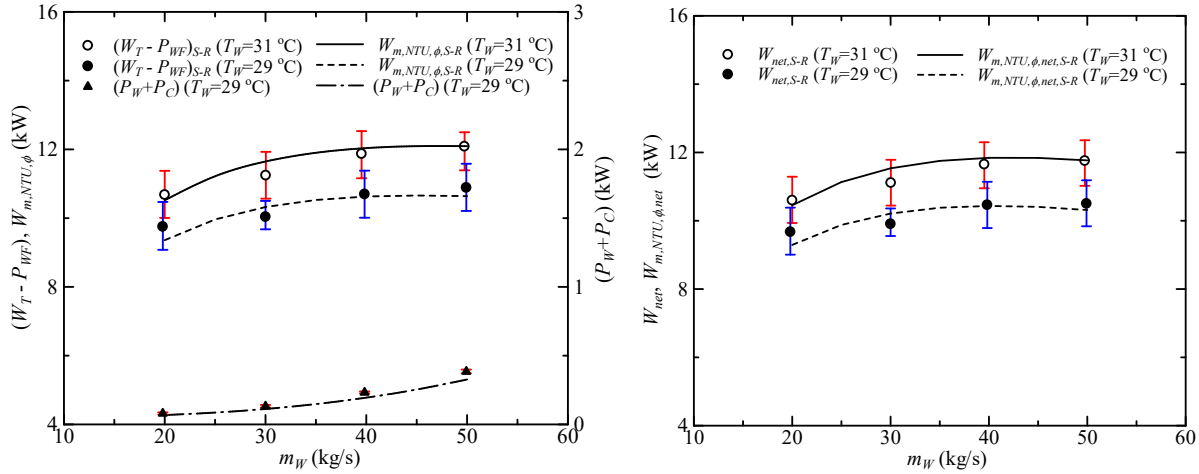

(a) Power from heat engine and pump workload (b) Net power

Figure 2: Experimental results for the power output of the heat engine, pumping power, and net power of the power generation system, and FTT model calculation results. The error bars are indicated for the experimental results to show the uncertainty.

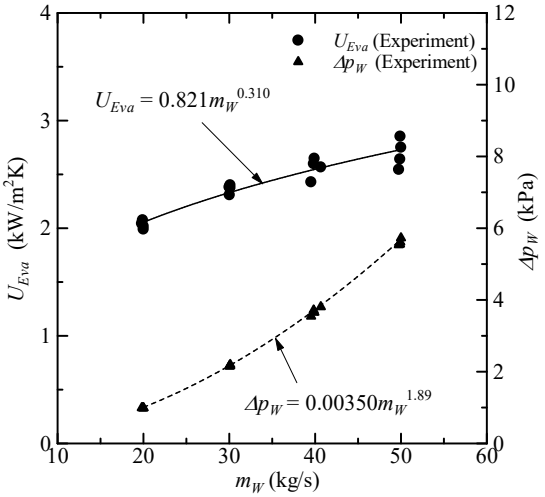

Figure 3: Experimental results for the evaporator overall heat transfer coefficient and pressure drop in the warm heat source side as a function of the mass flow rate of the warm heat source.

$$\Delta p_W = 0.0350 m_W{}^{1.89} \tag{18}$$

By comparing the experimental heat engine power output with the findings obtained using Equation (8) by assuming that the each operating point is a maximum power condition, ϕ can be calculated by minimizing the difference between the results obtained using Equation (8) and (W_T - P_{WF}), i.e., Min.$\left|W_{m,NTU,\phi} - (W_T - P_{WF})\right|$. The following simplified empirical formula of ϕ can express almost all the data within an error of 3%:

$$\phi = 0.9692 \varepsilon_{Eva}{}^{0.20} (\sqrt{T_W} - \sqrt{T_C})^{-0.037} \tag{19}$$

Using Equations (8) and (17)–(19), the net power output can be predicted based on the FTT model. The calculation results are shown in Figure 2. According to Figure 2, the agreement within the uncertainty of the experimental results was obtained between the calculation and experiment. The FTT model provides the optimum operating condition that can maximize the net power output in the warm heat source, specifically, m_W=42.3 kg/s.

4.2 Effect of Staging Based on the FTT Model

The FTT model established in section 4.1 using a single Rankine cycle (S-R) is extended to the cascade double-stage Rankine cycle heat engine (D-R) and double-capacity (parallel two unit) Rankine cycle

(DC-R) to compare the effectiveness of staging (Shown in Figure 4). Figure 5 shows the net power output and exergy efficiency of S-R, D-R, and DC-R calculated using the FTT model. In the D-R case, the intermediate heat source temperatures for each heat source, outlet of the evaporator in the first-stage Rankine cycle, and outlet of the condenser in the second-stage Rankine cycle, are calculated using the FTT model for each stage. In the DC-R case, the heat transfer area is two times that in the single Rankine case; however, the mean velocity in the heat exchanger is half of that in the former case. Thus, the overall heat transfer coefficient of the evaporator is calculated using Equation (17) as a function of the mean velocity of the heat exchanger, and the dependence of the overall heat transfer coefficient of the condenser is assumed to be the same as that of the evaporator. In Figure 5, the black, red, and blue lines correspond to S-R, D-R, and DC-R, respectively; and the solid and dashed lines correspond to the conditions of T_W=29 and 30 °C, respectively. According to Figure 5(a), the net power is significantly increased owing to the staging: The net power of D-R is approximately 1.5 times that of S-R. Although the two-stage Carnot heat engine has a maximum power output that is 1.3 times higher than that of the single stage (Yasunaga and Ikegami, 2020a), the net power of the FTT model exhibits a considerable increase by staging. The primary reason for the significant increase is the approximation formula of the overall irreversibility in Eq. (19), of which the temperature difference between inlet warm water and cold water is the function. Then, the decrease of the irreversibility in each cycle in D-R leads to the remarkable increase of the net power. In contrast, in the case of DC-R, the increase in the net power is only 23.0–47.7%. If the heat source flow rates are two times those of S-R, the net power increases by two times, although the exergy efficiency is significantly smaller because the exergy depends on the total heat source flow rate. The exergy in the D-R exhibits a notable improvement of 62.8–67.4%, as shown in Figure 5(b), although the corresponding value in the DC-R case is only 23.0–47.7% higher than that of the S-R. The exergy increase in the D-R case is significant because the theoretical maximum

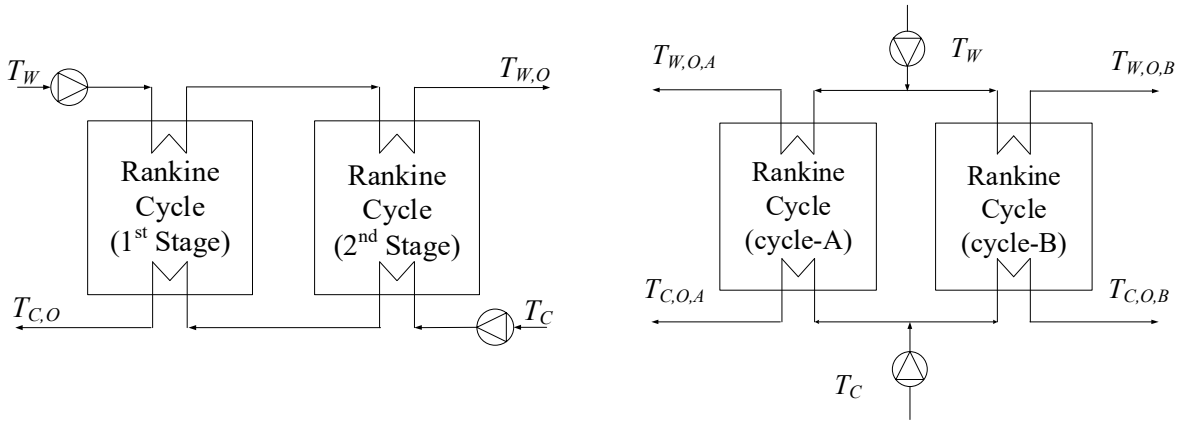

(a) cascade double stage Rankine cycle (D-R) **(b)** double-capacity Rankine cycle (DC-R)

Figure 4: Conceptual flow diagram of double stage or double capacity Rankine cycle.

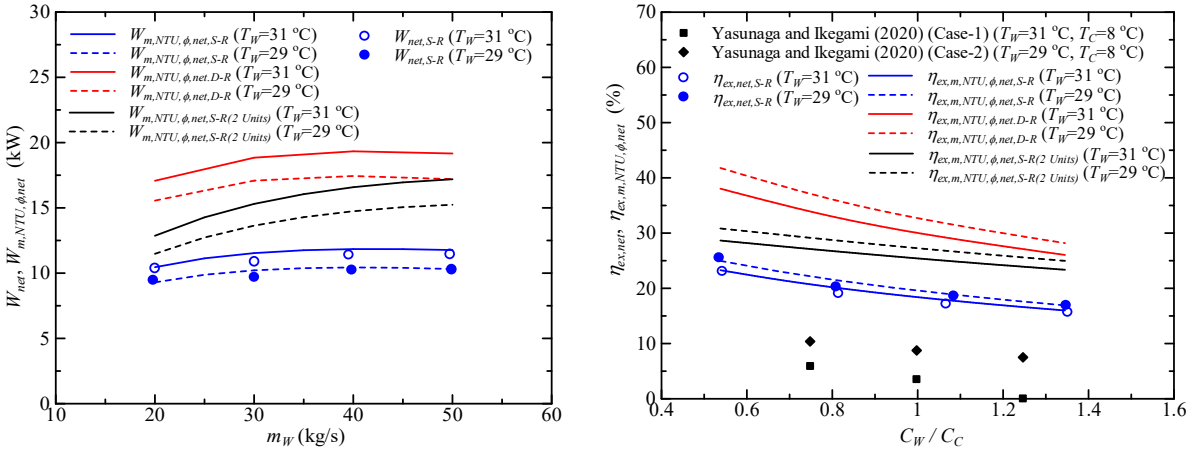

(a) Net power output (b) Exergy efficiency

Figure 5: Net power output and exergy efficiency of the S-R, D-R, and DC-R cases.

exergy of the single Carnot cycle is 50% (Yasunaga and Ikegami, 2020a). Another advantage of the D-R configuration is that the seawater intake piping is the same size as that of the single Rankine cycle, which leads to a high cost effectiveness. Figure 5(b) shows the 30 kW OTEC test results (Yasunaga and Ikegami, 2020b). The exergy efficiency obtained in this work is higher than that pertaining to 30 kW testing.

5 CONCLUSIONS

An FTT model is constructed based on the experimental data to analyze the irreversibility of a heat engine. This model consists of the degradation of the maximum available work in the reversible het engine due to finite heat transfer performance of the heat exchangers, finite performance of the component of the heat engine such as turbine and working fluid pump. The benefit of the model is analyzable the effect of the performance of the components on the net power, and not required the complicated calculations of the heat and mass balance and applicable to the operation and control to maximize the available power. The constructed model in the current research clarifies the optimum heat source flow rate to maximize the net power in the case of a single Rankine cycle. Furthermore, the model is extended to compare the double-stage to simulate the effectiveness of the staging of the heat engine in terms of the net power and the exergy efficiency. The results demonstrate the effectiveness of the FTT model and potential for application to ensure optimum control and design.
For the future work, firstly, the difference between conventional exergy analysis and current FTT model analysis should be clarified. And, because the exergoeconomic point of view is necessity for the engineering, the application of FTT model to the thermoeconomics analysis should be performed.

NOMENCLATURE

A	heat transfer area of the heat exchanger	(m^2)
C	heat capacity	(kW/K)
h	specific enthalpy	(kJ/kg)
m	mass flow rate	(kg/s)
P	pump workload	(kW)
Δp	pressure difference	(kPa)
S	entropy	(kJ/K)
T	temperature	(K)
U	overall heat transfer coefficient	(kW/m^2K)
ε	effectiveness of the heat transfer performance	(-)
ΔT_m	logarithmic mean temperature	(K)
ϕ	irreversibility coefficient	(-)
η	efficiency	(%)
ρ	density	(kg/m^3)
Subscript		
C	cold source	
Con	condenser	
Eva	evaporator	
HS	heat source	
I	inlet	
m	maximum	
net	net	
O	outlet	
T	turbine	
W	warm source	
WF	working fluid	

REFERENCES

Avery, W. H, Wu, C., 1994, Renewable energy from the ocean a guide to OTEC, Oxford University Press, New York, pp.98-101.

Bejan, A., 2016, Advanced engineering thermodynamics, John Wiley & Sons, 4th Edition, New Jersey, pp. 95-139

Curzon, F. L., Ahlborn, B., 1975, Efficiency of a Carnot engine at maximum power output, *Am. J. Phys.*, vol.43, no.22, pp.22-24.

Dincer, I., Rosen, M. A., 2021, Exergy, Elservier, Netherlands, pp. 527-563.

Fontaine, K., Yasunaga, T. and Ikegami, Y., 2019, OTEC maximum net power output using Carnot cycle and application to simplify heat exchanger selection, *Entropy*, vol.21, no.12, p.1143.

Ibrahim, O. M., Klein, S. A. and Mitchell, J. W.,1991, Optimum heat power cycles for specified boundary conditions, *J. Eng. Gas Turbines Power*, vol.113, pp.514-521.

IEA-OES, 2019, Annual report. an overview of ocean energy activities in 2019.

Ikegami, Y., Bejan, A., 1998, On the thermodynamic optimization of power plants with heat transfer a fluid flow irreversibilities, *J. Sol. Energy Eng.*, vol.120, no.2, pp.134-144.

Ikegami, T., Yasunaga, T., Morisaki, T., 2018, Ocean Thermal Energy Conversion Using Double-Stage Rankine Cycle, *J. Mar. Sci. Eng.*, vol. 6, no.2, p.21.

Kalina, A.L. 1984, Combined cycle system with novel bottoming cycle, *J. Eng. Gas Turbines Power*, vol. 106, pp.737–742.

Lemmon, E. W., Bell, I. H., Huber, M. L. and McLinden, M. O., 2018, NIST Standard Reference Database 23, NIST REFPROP Version 10.0.

Martin, B., Okamura, S., Nakamura, Y., Yasunaga, T., Ikegami, Y., 2016, Status of the "Kumejima Model" for advanced deep seawater utilization, *Proc. IEE Conf. Pub.*, pp. 211-216.

Owens, W. L., 1983, Optimization of closed-cycle OTEC plants. *Proc. ASME-JSME Therm. Eng. Jt. Conf.*, vol.2, pp.227-239.

Talluri, L., manfrida, G., Ciappi, L., 2021, Exergo-economic assessment of OTEC power generation, *E3S Web of Conference*, vol. 238, p.01015.

Uehara, H., Ikegami, Y., 1990, Optimization of a Closed-Cycle OTEC System, *J. Sol. Energy Eng.*, vol.112, pp. 247–256.

Uehara, H., Ikegami, Y., Nishida, T., 1995, OTEC system using a new cycle with Absorption and Extraction Process, *Phys. Chem. Aqueous Sys.*, pp. 862–869.

Uehara, H.; Nakaoka, T., 1985, OTEC Plant Consisting of Plate Type Heat Exchangers, *Heat Transf. Jpn. Res.*, vol.14, pp.19-35.

Uehara, H.; Nakaoka, T., 1987, OTEC for Small Island, *Sol. Eng.*, vol.2, pp.1029-1034.

Yasunaga, T., Fontaine, K., Ikegami, Y., 2021, Performance evaluation concept in ocean thermal energy conversion towards standardization and intelligent design, *Energies*, In press.

Yasunaga, T., Ikegami, Y., 2019, Irreversibility in the organic Rankine cycle for low-grade thermal energy conversion system, *Proc. 5th Int. Seminar ORC Power Systems*, p.162.

Yasunaga, T., Ikegami, Y., 2020a, Finite-Time Thermodynamic Model for Evaluating Heat Engines in Ocean Thermal Energy Conversion, *Entropy*, vol.22, no.2, p.211.

Yasunaga, T., Ikegami, Y., 2020b, Theoretical model construction for renewable low-grade thermal energy conversion: an insight from finite-time thermodynamics, *Proc. IIR Rankine 2020*, no.1185.

Yasunaga, T., Noguchi, T., Morisaki, T., Ikegami, Y., 2018, Basic Heat Exchange Performance Evaluation Method on OTEC, *J. Mar. Sci. Eng.*, vol.6, no.2, p.32.

Vera, D., Baccioli, A., Jurado, F., Desideri, U., 2020, Modeling and optimization of an ocean thermal energy conversion system for remote islands electrification, *Renew. Energy*, Vol. 162, pp.1399-1414.

Wu, C., 1987, Performance Bound for Real OTEC Heat Engines, *Ocean Eng.*, vol. 14, pp. 349–354.

ACKNOWLEDGEMENT

This research was supported by JSPS KAKENHI Grant number JP20K04313 and Science and Technology Research Partnership for Sustainable Development (SATREPS) in collaboration between Japan Science and Technology Agency (JST, JPMJSA1803) and Japan International Cooperation Agency (JICA).